SYNTHESIS OF BINARY METAL NANOPARTICLES OF Ru-Ni WITH CORE AND SHELL STRUCTURE

Kalyana C. Pingali, Shuguang Deng, David A. Rockstraw

Department of Chemical Engineering, College of Engineering

New Mexico State University, P.O. Box 30001, MSC 3449, Las Cruces, NM 88003

Abstract

Binary metal nanoparticles of Ru-Ni were synthesized with core and shell nanostructures by flash pyrolysis. Ruthenium chloride and Nickel chloride were used as a binary mixture to generate the binary nanoparticles. SEM and TEM images confirmed the formation of eutectic metal deposits of less than 15 nm with Ruthenium forming the core and Nickel forming the shell and Ru-Ni binary metal core and shell nanostructure was obtained. Characterization of the nanoparticle size was achieved by fit to a log-normal distribution. X-ray images of the samples taken also confirmed the concentration of ruthenium more at the core of the particle.

1.0 Introduction

Nanoparticles of Ru-Ni synthesized from binary solutions can be used as catalysts in the fuel cell applications. We have earlier demonstrated the synthesis of nanoparticles of Ru, Ni by flash pyrolysis in the size range of less than 20 nm. Various studies have been carried out in the synthesis of binary metal nanoparticles in the past. Xiang [1] used binary organic solvent diffusion technique to synthesize nanoparticles of polylactide (PLA) and poly(lactide-co-glycolide) (PLGA) to evaluate the yield, size and size distribution. Yield of over 90% with an average size of 130-180 nm was obtained and the effect of organic solvent on the yield was investigated. Papp [2] used solid/liquid interfacial as a nanoreactor where Pd-O nanoparticles are synthesized by growth in the internal and external space of lamellae.

Structural phase studies of metallic and bimetallic nanoparticles were studied. Hills [3] condensed one metal precursor onto pre-supported nanoparticles of a second metal in the synthesis of binary nanoparticles of Pt-Ru. It was observed that the second metal acted as a nucleating site for the growth of binary phase. Crystalline growth was seen as a reason for the synthesis of powders of binary metals. Li [4] used binary carbonaceous titania aerogel in the preparation of Ti (C,N,O) and observed that carbothermal reduction temperature was vital for the crystalline growth of Ti (C,N,O) powders. Control factors governing the formation of bimetallic nanoparticles are vital in the structural analysis of binary nanoparticles. Kariuki [5] investigated the synthesis of monolayer-capped binary gold-silver (Au-Ag) bimetallic nanoparticle. Correlation was developed between the synthetic feeding of metals and metal compositions in the binary nanoparticles. A two phase reduction was observed in this case.

Alloys of various metal compositions were prepared in the past to study the catalytic activity. Research on the growth process and phase diagrams were crucial in the structural study of the binary metal systems. Takatani [6] prepared Au-Pd alloy nanoparticles by ultrasound irradiation of solutions. Electronic state of Au-Pd alloy was studied. Onho [7] studied the morphology of immiscible binary nanoparticles of Si-In, Ge-In, Al-In and Al-Pb by using X-Y composite nanoparticles of four immiscible binary systems by the condensation of Y vapor onto X nanoparticles through a gas-evaporation technique. Phase diagrams were used to describe their growth process. A homogeneous

distribution of all the metal particle systems was observed in all the above cases. The distribution of the two particles into one metal system is of vital importance.

Integration of different materials with varying properties into a composite metal system is of interest to various technical and scientific applications. Coowanitwong [8] used a dry metallic coating technique to get a well dispersed and homogeneous distribution of Al2O3 and CuO nanoparticles. It was observed that the particle loading increased the product surface area. Izgaliev [9] synthesized alloys of Au and Ag and observed that concentration of nanoparticles and surfactants in the mixture was related to the rate of alloy formation. Formation of core and shell of nanoparticle explains the structure of binary nanoparticle. Nakanishi [10] produced core shell structured bimetallic Au/Pt alloy nanoparticles. It was observed that the structures of nanoparticles changed with surfactant. Todaka [11] observed that the Fe-Cu and Fe-Ag nanoparticles were super saturated solid solutions with the growth of whiskers on their tip as the result of the phase separation in solid solutions.

Formation of alloys in the sub-nano range can be considered crucial in the formation of alloys that are required for the applications of fuel cell catalysts. Size of the nanoparticle can have an effect on the composition of thebulk alloy. According to Jayaganthan [12], surface compositions in the Ni-Co binary alloy single-crystal nanoparticles are larger than that of the corresponding bulk single crystal. This was observed to be true with particle diameter of 10-100 nm when compared to bulk crystals of > 100 nm. The thermodynamics of structure of binary system was studied. Interface of these structures with other useful nanoscale building blocks can were studied by Zhu [13]. The synthesis of binary nanomaterials was made from single-walled nanohorns. This may form the key area to explain the formation of different nanoparticles in a single binary alloy. Efforts were made to explain the binary structures.

Binary nanoparticles were synthesized not only from binary solutions but also from bimetallic nanoparticles. Lang [14] prepared supported Pt-Au catalysts from bimetallic dendrimer-stabilized nanoparticles (DSNs). Stability of the phase with core-shell structure is important in understanding the phase confirmations and thermal behavior. This was investigated by Rodriguez-Lopez [15], by studying the Au-Cu binary cluster to understand the thermal behavior and phase confirmations and observed a quasi-spherical shape of within a core at high temperature, just before the melting temperature of the cluster. Kim [16] studied the electrochemical and catalytic activities of Ni, Ru, and Ru-Ni by electron deposition. When compared to that of the bulk metals, it was observed that the Ru-Ni nanoparticles are more effective catalysts for ethanol oxidation. G4 (NH_2) and G5 (OH) dendrimers were used in the electrochemical deposition of ruthenium and nickel to enhance the oxidation properties of organic compounds.

In the case of eutectics solutions, for small particles in the size range of nanometers, the phase diagram of such small particles needs to be studied in order to understand the effect of size. Vallee [17] deduced that the phase diagram of small particles is a function of their size within the limits of thermodynamic arguments. Sulitanu [18] observed that by changing the metallic ion concentration, the metallic elements concentration can be

controlled in the synthesis of amorphous ultra-fine powders in (Fe, Co, Ni)-B binary and ternary systems by chemical reduction method. According to Santra [19], nucleation and growth on empty sites depend on availability of empty-step sites. The growth of Ag-Au bimetallic nanoparticles on TiO_2 was studied and was observed that these bimetallic nanoparticles are of alloy type rather than core-shell type. Demydov [20] used a modified aerogel procedure to synthesize nanosized mixed-metal-oxide particles of strontium and barium titanate (SrTiO3 and BaTiO3).

Over the years several binary metal oxides, alloys have been synthesized, and their properties and structures have been studied. In this paper, we try to investigate the possibility of formation of binary metal nanoparticle with core and shell nanostructure. An attempt was made to synthesize bimetallic nanoparticles in the size of less than 15 nm. Experimental and operating conditions were adjusted for the depositions of metals accordingly. Binary solutions of ruthenium chloride and nickel chloride were used to make bimetallic nanoparticles of Ru-Ni. An attempt was made to form binary phases metal phases of Ru and Ni. Synthesis of Ru-Ni nanoparticles by spray pyrolysis in the size range of less than 15 nm was not done before at low concentrations. An attempt is made in this work to combine these factors to synthesize binary metal nanoparticles by flash pyrolysis to form a core and shell structure of deposits on the substrate.

2.0 Experimental Method

The experiments were carried out in flash pyrolysis equipment set up. Thermal disintegration of the aqueous solutions can result in metal deposits of Ru-Ni binary nanoparticles on the substrate kept at the bottom of the reactor on a sample holder. Binary solution mixture of ruthenium chloride and nickel chloride was used as a feed solution. The aqueous binary solution was gravity fed to the atomizer which nebulizes the liquid with ultrasonic frequency. The frequency of ultrasonic atomizer can be adjusted with the variation of the input power to the atomizer. A reactor tube was used as the reaction chamber where the thermal disintegration of the aqueous solution takes place at high temperature. A reactor furnace was used to supply the heat required for pyrolysis temperature below the melting point of the metals. Argon was used as a carrier gas to entrain the metal deposits.

The initial set of experiments were carried out at a feed solution concentration of 10^{-2}N, with an input atomizer power at 5W at a pyrolysis temperature of 700°C. The second set of experiments were carried out at a feed solution concentration of 10^{-4}N, with an input atomizer power at 5W at a pyrolysis temperature of 700°C. This was done to check the effect of fed solution concentration on the binary mixtures and binary nanoparticle size distributions. Therefore, atomizer power and the reactor temperature temperature were kept constant by varying the feed solution concentration from 10^{-2}N to 10^{-4}N. Since the structure of the binary nanoparticles cannot be judged on TEM except for the size, the concentration of the solution was increased to 10^{-1}N, in order to obtain bigger particles. This was done to study the structure of the composite binary metal nanoparticles in the samples collected.

The final set of experiments were run with binary mixture solution concentration of 10^{-1}N, atomizer power at 4.5 W and reactor temperature of 750°C. The solutions were prepared by dissolving the ruthenium chloride and nickel chloride in deionized water. This experiment was done to obtain an image for X-ray diffraction to check the population of nickel and ruthenium inside the binary nanoparticle. The characterization of the samples was done with SEM, TEM and XRD images and graphs. The size of the particles was calculated by counting the individual particles obtained from TEM images and fitting to a particle size log-normal distribution.

3.0 Mechanism

The deposition of samples of nanoparticles is expected by the evaporation of the liquid droplet. A binary feed solution when passed through the atomizer, the aerosol generated by the ultrasonic atomizer due to the ultrasonic frequency generates aerosol bubbles. Each bubble contains the binary particles of ruthenium and nickel. Evaporation of the droplet can result in the deposition of the bubble constituents. Since the bubble contains a binary solution, evaporation of the aqueous phase can result in the deposition of the binary particles of ruthenium and nickel together into a single particle.

The eutectic composition and transition temperature differ from those of the bulk when the size of the components decreases to nanometric size range. Melting point of ruthenium is 2310°C and that of nickel is 1453°C. Since the melting point of nickel is less than that of ruthenium, the molecular forces of attraction or molecular bonding might be week for nickel. In case of Ru-Ni, the particles in aerosols are deposited as nanoparticles of Ru-Ni by evaporating the aqueous aerosol phase by high temperature in the reactor. When this happens, the bulk phase of the particles in aerosols decreases to the nanometric size range. Chemical environments play a vital role in determining the size and structure of nanoparticle. Stoichiometry of the core and the stoichiometry of the surface in the binary nanoparticle depend upon the number of atoms. According to Vallee [21], phase diagrams of small particles in nanometric range are the function of their size. It is well known that the particles in the size range of 1-100 nm are in the intermediate state between solid and molecular state. When the number of atoms in a particle are 1000 and above, the particle changes from molecular to solid form. Thus the surface to volume ratio of atoms is vital in explaining the structure of a binary nanoparticle. Thus, the surface has an impact over the cohesive property of the particle.

As the size decreases, the melting temperatures of both the components in a binary mixture decreases and a eutectic melting point is much lower than that of the individual components. It was assumed that the ruthenium chloride and nickel chloride mixture is a bulk phase. As the size of the component decreases from liquidus form to solidus form, the atomic composition decreases. The bulk phase of the components are reduced to the nanosize range in case of ruthenium and nickel. Recent works on the nanoparticles indicate that the structure of nanoparticle is not uniform. This hypothesis was studied by Edelstein [22] for Cu-Co nanocrystals, and Ramos [23] for Ni-Al nanoparticles. They found that there is a difference of the binary nanoparticle structure when compared to that of the bulk phase. It was found that the binary nanoparticles can accommodate structural defects on the cluster surface. These defects are introduced by

the stoichiometry deviations. These structures represent a highly ordered core surrounded by a chemically disordered mantle.

It was found that the surface segregation results in a new repartition of atomic species between core and surface. This can be applicable where the shape does not change with size of the particle. The stoichiometry of the core and the stoichiometry of the surface depend on the number of atoms in the binary system. In the case of a binary nanoparticle of Ru-Ni, Ru has higher heat of vaporization due to its higher melting point. Therefore, nickel can be expected to distribute at the outer surface due to weaker molecular forces when compared to ruthenium. Due to the high heat of vaporization and higher melting point than nickel, stronger molecular forces of ruthenium can result in a metal deposit with ruthenium forming the core. This can result in a highly ordered core of ruthenium and chemically disordered nickel at the surface of the binary nanoparticle of Ru-Ni in the final deposits.

The phase diagrams of the bulk solutions vary to that of the nanoparticles and atomic composition of the solution. As the size is reduced to nanometric range, the nanoparticle may behave as a eutectic where the melting temperature of the binary nanocomponent is different to that of the bulk phase composition. The melting temperature of the components in the bulk phase may decrease with the size of the particle. The decrease in size can result in the decrease in melting temperature of the metal components. The nickel nanoparticles due to the weak molecular forces of attraction, can be expected to reach the stage of loosely bonded, and can be expected to be deposited at the surface of the particle. Though the melting point of ruthenium decreases from bulk to nanoparticle size range, this can still be considered to be higher than nickel with stronger forces of molecular attractions. Therefore, ruthenium can be expected to form the core of binary nanoparticle.

4.0 Results and Discussion

The result of the initial first batch of the experiment can be seen in Figure 1 and Figure 2. This shows a TEM image of the set of experiments ran at a feed solution concentration of 10^{-2}N, with an input atomizer power at 5W at a pyrolysis temperature of 700°C. It can observed that the average size of Ru-Ni binary particles was in the size range of 22.69 nm with a standard deviation of 6.11. A total of 49 particles were counted on this TEM image. Figure 3 and Figure 4 show a TEM image of the set of experiments ran at a feed solution concentration of 10^{-4}N, with an input atomizer power at 5W at a pyrolysis temperature of 700°C. The other two operating conditions of reactor temperature and atomizer power were kept constant and concentration was decreased to see the effect of feed solution concentration on the average binary nanoparticle size. A total of 57 particles were counted on this TEM image. The average particle size of Ru-Ni binary nanoparticle was observed to be 11.52 nm with a standard deviation of 3.8. A low standard deviation shows a good particle size distribution. The tabulated results can be seen from Table 1.

The particle size was determined from the TEM images, but this could not show whether the particles of Ru-Ni were deposited separately or as a single particle as a

binary nanoparticle. To evaluate this, nanaoparticle size was increased beyond 100 nm to be clearly seen on SEM. The concentration was increased to increase the size and for the particles to be clearly seen on the SEM. Figure 5 and Figure 6 show the SEM image of the particle size distribution of the batch of experiment carried out at a feed solution concentration of 10^{-1}N with atomizer power of 5W and the reactor temperature at 700°C. It can be clearly seen from Figure 5 that the binary nanoparticles are formed in a core and shell structure. This phenomena was observed to be true for every particle on the size distribution.

The spectral analysis was done to evaluate the constituent particles of the samples. It was observed that the inside core was formed by ruthenium and nickel formed the outer shell. An overall spectral analysis was done. The spectral analysis was also done at particular point in the nanoparticles. A point was selected at the shell and the spectra analysis was evaluated. A similar point analysis was done at the core of the particle. Though ruthenium and nickel were present in both the peaks at both points analyzed, the concentration of ruthenium deposition was more at the center of the particle, and nickel concentration was considerably less at the shell surface of the particle. The SEM images show a uniform particle size distribution with a clear separation of phases inside the nanoparticles.

X-ray imaging was also done to evaluate and study the constituents of the binary nanoparticles of ruthenium and nickel. To evaluate this, a set of experiments was run with binary mixture solution concentration of 10^{-1}N, atomizer power at 4.5 W and reactor temperature of 750°C. Figure 7 show a SEM image of a particle selected to check for X-ray imaging. It can be clearly seen from this image, that the particle is forming a shell and core structure. Figure 7 confirms the deposition of the binary particle with a thick ring -like shell at the surface and a thick core at the inside. An over all X-ray imaging was done to study the particle population or constituency in this image. An overall imaging was done initially to see the particle concentration. Figure 8 shows the overall X-ray image of the binary nanoparticle of Ru-Ni of particle which can be seen from Figure 7. The overall image shows that the ruthenium concentration is more at the center. This confirms the mechanism discussed earlier that the deposition of the ruthenium will be at the core due to the higher melting point and stronger forces of inter molecular attractions. It can also be seen from Figure 8 that the nickel deposits are less than the core than ruthenium as can be seen separately. Figure 9 shows the overall spectra image of ruthenium and nickel inside the nanoparticle.

A point analysis was also done to evaluate the constituent binary nanoparticles. A single point was selected at the center core of the particle and X- ray of that particular point was taken. It can be seen from Figure 10 that the population of ruthenium particles is more than the nickel nanoparticles. A separate X-ray imaging can be seen both for ruthenium and nickel in two separate windows. This also confirms the mechanism discussed earlier that the concentration of ruthenium would be more at the center forming the core with a nickel shell on the outer ring of the binary nanoparticle.

To confirm the above trends of ruthenium and nickel, another image of X-ray was taken for a sample obtained. The operating conditions for this experiment were similar to

that of the previous one. Figure 10 shows the SEM image of the binary nanoparticle. This sample was obtained when the experiment was repeated with similar set of operating conditions. Figure 11 shows the X-ray image of this binary nanoparticle. It can also be seen from Figure 11 that the ruthenium is deposited inside the core and nickel formed an outside shell of the particle. It can be seen from Figure 11 that the ruthenium at the center takes the shape of the inner core which can be seen from the overall imaging of the nanoparticle towards the right side of the X-ray image. It can also be seen that the ruthenium is more at the core and nickel deposited at the shell. Figure 12 shows the X-ray imaging of the binary nanoparticle at a center point inside the core of the nanoparticle. Figure 13 shows the spectra image of the overall nanoparticle with the presence of ruthenium and nickel inside the binary nanoparticle.

5.0 Conclusions

Binary solution mixtures of ruthenium chloride and nickel chloride can be used synthesize the binary nanoparticles of ruthenium and nickel by flash pyrolysis. Thermal disintegration of the solution of ruthenium chloride and nickel chloride resulted in a binary Ru-Ni nanoparticle with ruthenium forming the core and nickel forming the shell of the particle. Binray metal nanaoparticles of Ru-Ni can be synthesized from binary mixture solutions of ruthenium chloride and nickel chloride.

(1) A clear distribution of ruthenium in the core and nickel in the shell can be obtained for every nanoparticle.
(2) The decrease in the concentration also resulted in the size of the binary nanoparticle.
(3) Though the ruthenium and nickel was present throughout the particle, the concentration of ruthenium was concentrated more at the core of the binary nanoparticle.
(4) The concentration of the core depended on the feed solution concentration of the binary mixture.

Nomenclature

˚ C	unit of relative temperature, degrees Celcius
nm	nanometer
TEM	Transmission Electron Microscopy
SEM	Scanning Electron Microscopy
N	unit of measurement of concentration, Normality
W	unit of power, watts

References

[1] X.Y.JIANG, C.S.ZHOU and K.W.TANG, Preparation of PLA and PLGA nanoparticles by binary organic solvent diffusion method, *Journal of Central South University of Technology*. **10**(3) (2003) 202-206.

[2] S.PAPP, A.SZUCS and I.DEKANY, Preparation of Pd-0 nanoparticles stabilized by polymers and layered silicate, *Applied Clay Science*. **19**(1-6) (2001) 155-172.

[3] C.W.HILLS, N.H.MACK and R.G.NUZZO, The size-dependent structural phase behaviors of supported bimetallic (Pt-Ru) nanoparticles, *Journal of Physical Chemistry*. **107**(12) (2003) 2626-26.

[4] X.K.LI, L.LIU, S.GE, S.D.SHEN, J.R.SONG, Y.X.ZHANG and P.H.LI, The preparation of Ti(C,N,O) nanoparticles using binary carbonaceous titania aerogel, *Carbon*. **39**(6) (2001) 827-833.

[5] N.N.KARIUKI, J.LUO, M.M.MAYE, S.A.HASSAN, T.MENARD, H.R.NASLUND, Y.H.LIN, C.M.WANG, M.H.ENGELHARD and C.J.ZHONG, Composition-controlled synthesis of bimetallic gold-silver nanoparticles, *Langmuir*. **20**(25) (2004) 11240-11246.

[6] H.TAKATANI, F.HORI, M.NAKANISHI and R.OSHIMA, Positron annihilation study on Au-Pd nanoparticles prepared by sonochemical technique, *Positron Annihilation, ICPA-13, Proceedings.* **445-4** (2004) 192-194.

[7] T.OHNO, Morphology of composite nanoparticles of immiscible binary systems prepared by gas-evaporation technique and subsequent vapor condensation, *Journal of Nanoparticle Research*. **4**(3) (2002) 255-260

[8] N.COOWANITWONG, C.Y.WU, M.CAI, M.RUTHKOSKY, J.ROGERS, L.FENG, S.WATANO and T.YOSHIDA, Surface modification of Al2O3 fiber with binary nanoparticles using a dry-mechanical coating technique, *Journal of Nanoparticle Research*. **5**(3-4) (2003) 247-258.

[9] A.T.IZGALIEV, A.V.SIMAKIN and G.A.SHAFEEV, Formation of the alloy of Au and Ag nanoparticles upon laser irradiation of the mixture of their colloidal solutions, *Quantum Electronics*. **34**(1) (2004) 47-50.

[10] M.NAKANISHI, H.TAKATANI, Y.KOBAYASHI, F.HORI, R.TANIGUCHI, A.IWASE and R.OSHIMA, Characterization of binary gold/platinum nanoparticles prepared by sonochemistry technique, *Applied Surface Science*. **241**(1-2) (2005) 209-212.

[11] Y.TODAKA, K.TSUCHIYA, M.UMEMOTO, M.SASAKI and D.IMAI, Growth of Fe3O4 whiskers from solid solution nanoparticles of Fe-Cu and Fe-Ag systems produced by DC plasma jet method, *Materials Science and Engineering A-Structural Properties Microstructure and Processing*. **15**(340) (2003) 114-122.

[12] R.JAYAGANTHAN and G.M.CHOW, Thermodynamics of surface compositional segregation in Ni-Co nanoparticles, *Materials Science and Engineering B-Solid State Materials for Advanced Technology*. **95**(2) (2002) 116-123.

[13] J.ZHU, D.KASE, K.SHIBA, D.KASUYA, M.YUDASAKA and S.LIJIMA, Binary nanomaterials based on nanocarbons: A case for probing carbon nanohorns' biorecognition properties, *Nano Letters*. **3**(8) (2003) 1033-1036.

[14] H.G.LANG, S.MALDONADO, K.J.STEVENSON and B.D.CHANDLER, Synthesis and characterization of dendrimer templated supported bimetallic Pt-Au nanoparticles, *Journal of the American Chemical Society*. **126**(40) (2004) 12949-12956.

[15] J.L.RODRIGUEZ-LOPEZ, J.M.MONTEJANO-CARRIZALES and M.JOSE-YACAMAN, Molecular dynamics study of bimetallic nanoparticles: the case of AuxCuy alloy clusters, *Applied Surface Science*. **219**(1-2) (2003) 56-63.

[16] J.W.KIM and S.M.PARK, Electrochemical preparation of Ru-Ni binary nanoparticles and their applications to electro-oxidation of ethanol, *Electrochemical and Solid State Letters*. **3**(8) (2000) 385-388.

[17] R.VALLEE, M.WAUTELET, J.P.DAUCHOT and M.HECH, Size and segregation effects on the phase diagrams of nanoparticles of binary systems, *Nanotechnology*. **12**(1) (2001) 68-74.

[18] N.SULITANU and I.SANDU, Synthesis using the chemical reduction method, microstructure and magnetic behaviour of ultra-fine amorphous powders in (Fe, Co, Ni)-B systems, *Revista De Chimie*. **54**(7) (2003) 561-565.

[19] A.K.SANTRA, F.YANG and D.W.GOODMAN, The growth of Ag-Au bimetallic nanoparticles on TiO2(110), *Surface Science*. **548**(1-3) (2004) 324-332.

[20] D.DEMYDOV and K.J.Kladunde, Characterization of mixed metal oxides ($SrTiO_3$ and $BaTiO_3$) synthesized by a modified aerogel procedure, *Journal of Non-Crystalline Solids*. **350** (2004) 165-172.

[21] R.VALLEE, M.WAUTELET, J.P.DAUCHOT and M.HECQ, Size and segregation effects on the phase diagrams of nanoparticles of binary systems, *Nanotechnology* **12** (2001) 68.

[22] A.S.EDELSTEIN, V.G.HARRIS, D.R.ROLISON, L.KURIHARA, D.J.SMITH, J.PEREPEZKO and M.H.DA SILVA BASSANI, *Applied Physics Letters*. **74** (1999) 3161.

[23] S.RAMOS DE DEBIAGGI, J.M.CAMPILLO and A.CARO, *Materials Research* . **14** (1999) 2849.

Acknowledgements

All the necessary and reactor system hardware was provided by LaSys Inc who has supported this project. Space Alliance Technology Outreach Program (SATOP) has provided the required financial support. Initial work on the reactor system was done by Dr. T.J. Mountziaris at State University of New York at Buffalo

Address

Correspondence concerning this paper should be addressed to Dr.David A. Rockstraw, Department of Chemical Engineering, College of Engineering, New Mexico State University, P.O. Box 30001, MSC 3449, Las Cruces, NM 88003. Tel: 505 6467705, Email: drockstr@nmsu.edu

Table Captions

Table1. Variation of binary nanoparticle size of Ru-Ni with feed solution concentration.

Table1. Variation of binary nanoparticle size of Ru-Ni with feed solution concentration

Experiment Number	Concentration (N)	Atomizer Power (W)	Temperature (°C)	Average Particle Size (nm)
01	10^{-2}	5	700	22.69
02	10^{-4}	5	700	11.52

Figure Captions

Figure 1. TEM image-1 of the binary nanoparticle of Ru-Ni carried out at a feed solution concentration of 10^{-2}N, with an input atomizer power at 5W at a pyrolysis temperature of 700°C

Figure 2. TEM image-2 of the binary nanoparticle of Ru-Ni carried out at a feed solution concentration of 10^{-2}N, with an input atomizer power at 5W at a pyrolysis temperature of 700°C

Figure 3. TEM image-1 of the binary nanoparticle of Ru-Ni carried out at a feed solution concentration of 10^{-4}N, with an input atomizer power at 5W at a pyrolysis temperature of 700°C.

Figure 4. TEM image-2 of the binary nanoparticle of Ru-Ni carried out at a feed solution concentration of 10^{-4}N, with an input atomizer power at 5W at a pyrolysis temperature of 700°C.

Figure 5. SEM image-1 of the particle size distribution of the batch of experiment carried out at a feed solution concentration of 10^{-1}N with atomizer power of 5W and the reactor temperature at 700°C.

Figure 6. SEM image-2 of the particle size distribution of the batch of experiment carried out at a feed solution concentration of 10^{-1}N with atomizer power of 5W and the reactor temperature at 700°C.

Figure 7. SEM image of a particle selected to check for X-ray imaging. This image confirms the deposition of the binary particle with a thick ring -like shell at the surface and a thick core at the inside.

Figure 8. Overall X-ray image of the binary nanoparticle of Ru-Ni of particle of the particle shown in Figure 7. It can be observed that the nickel deposits are less than the core than ruthenium.

Figure 9. Overall spectra image of ruthenium and nickel inside the nanoparticle.

Figure 10. SEM image of the binary nanoparticle with synthesized with conditions similar to the one shown in Figure 7.

Figure 11. X-ray image of binary nanoparticle shown in Figure 10. It can be observed that the ruthenium is deposited inside the core and nickel formed an outside shell of the particle. Ruthenium at the center takes the shape of the inner core which can be seen from the overall imaging of the nanoparticle towards the right side of the X-ray image.
Figure 12. X-ray imaging of the binary nanoparticle at a center point inside the core of the nanoparticle. It can be observed that the population of ruthenium particles is more than the nickel nanoparticles.

Figure 13. Spectra image of the overall nanoparticle shown in Figure 7. This confirms the presence of ruthenium and nickel inside the binary nanoparticle.

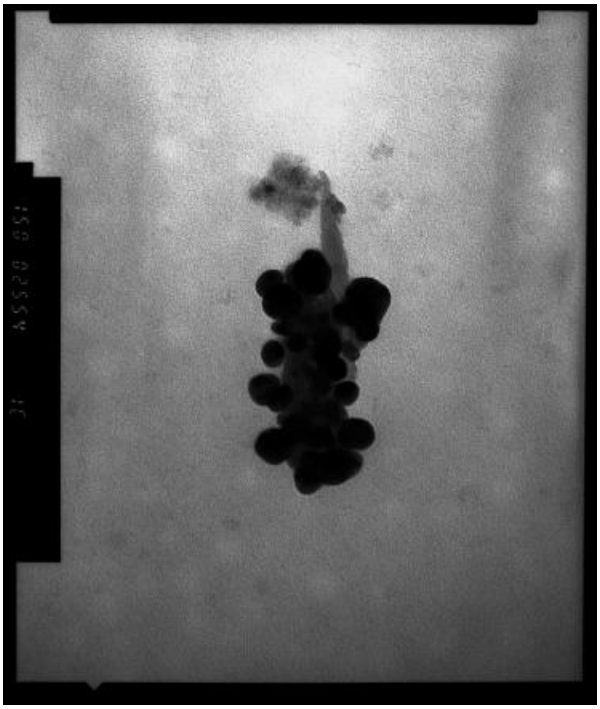

Figure 1. TEM image-1 of the binary nanoparticle of Ru-Ni carried out at a feed solution concentration of 10^{-2}N, with an input atomizer power at 5W at a pyrolysis temperature of 700°C

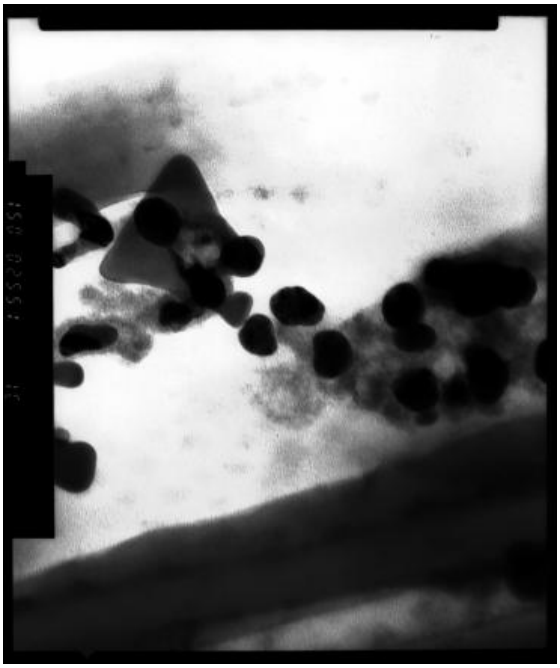

Figure 2. TEM image-2 of the binary nanoparticle of Ru-Ni carried out at a feed solution concentration of 10^{-2}N, with an input atomizer power at 5W at a pyrolysis temperature of 700°C

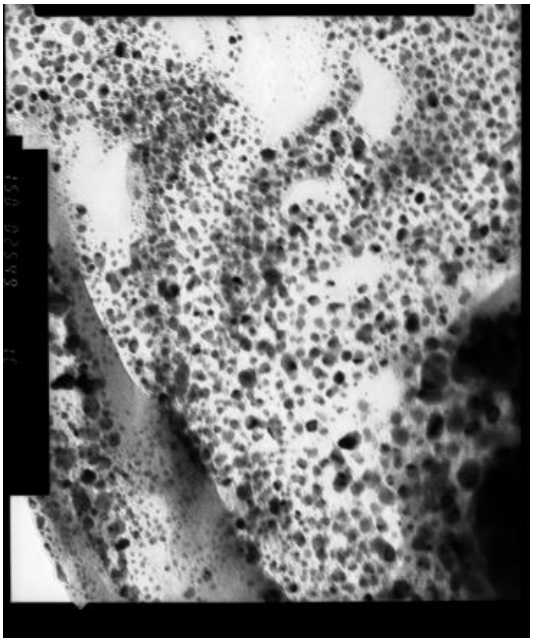

Figure 3. TEM image-1 of the binary nanoparticle of Ru-Ni carried out at a feed solution concentration of 10^{-4}N, with an input atomizer power at 5W at a pyrolysis temperature of 700°C.

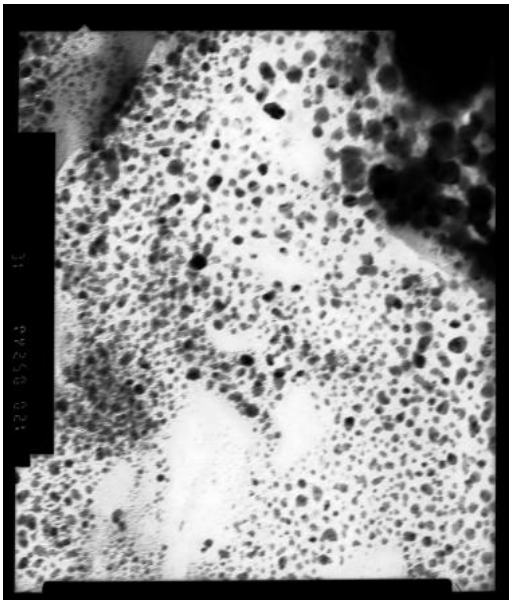

Figure 4. TEM image-2 of the binary nanoparticle of Ru-Ni carried out at a feed solution concentration of 10^{-4}N, with an input atomizer power at 5W at a pyrolysis temperature of 700°C.

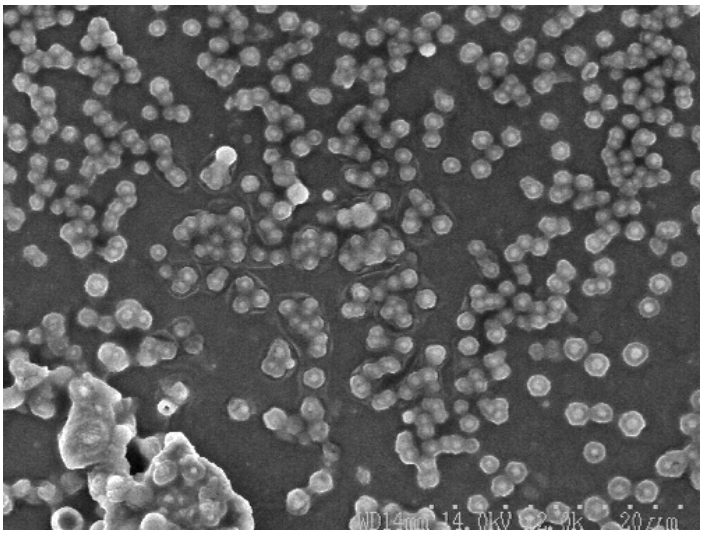

Figure 5. SEM image-1 of the particle size distribution of the batch of experiment carried out at a feed solution concentration of 10^{-1}N with atomizer power of 5W and the reactor temperature at 700°C.

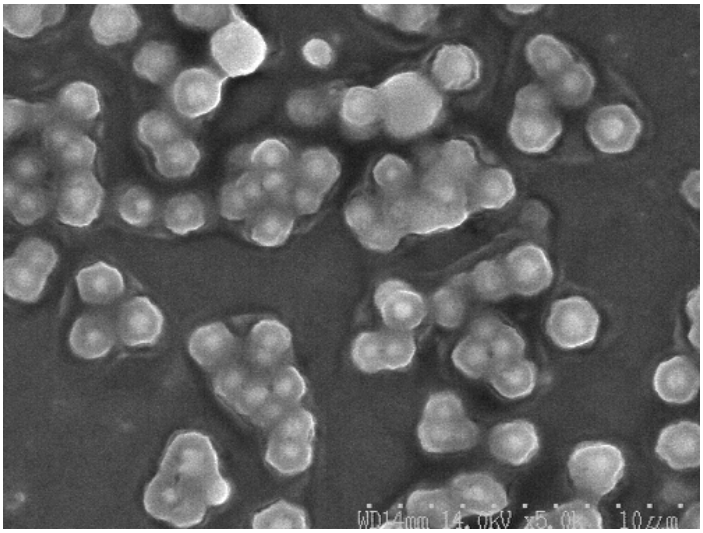

Figure 6. SEM image-2 of the particle size distribution of the batch of experiment carried out at a feed solution concentration of 10^{-1}N with atomizer power of 5W and the reactor temperature at 700°C.

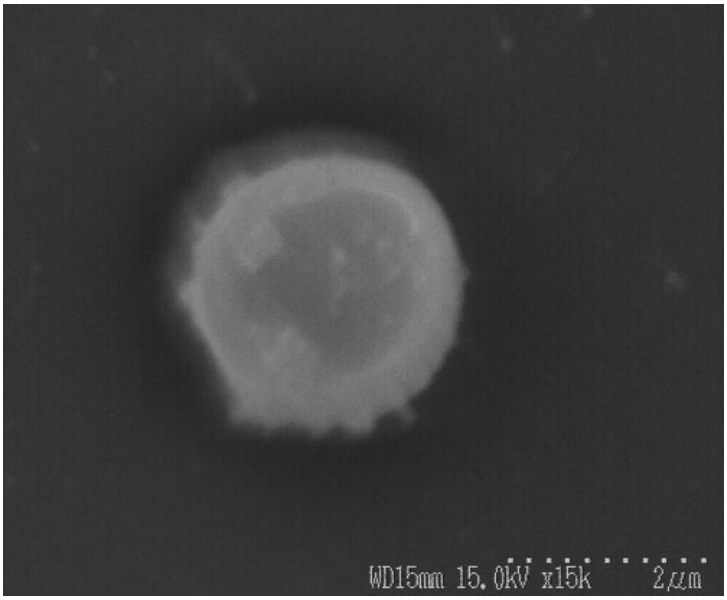

Figure 7. SEM image of a particle selected to check for X-ray imaging. This image confirms the deposition of the binary particle with a thick ring -like shell at the surface and a thick core at the inside.

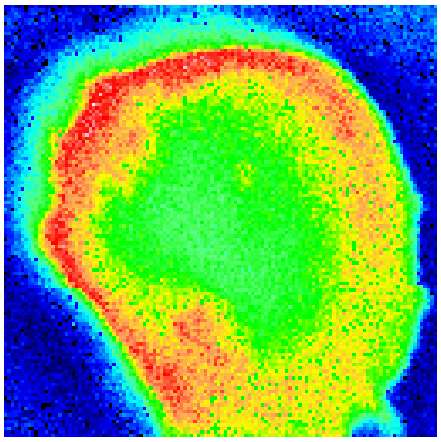

Figure 8. Overall X-ray image of the binary nanoparticle of Ru-Ni of particle of the particle shown in Figure 7. It can be observed that the nickel deposits are less than the core than ruthenium.

Nickel overall

Ruthenium (overall)

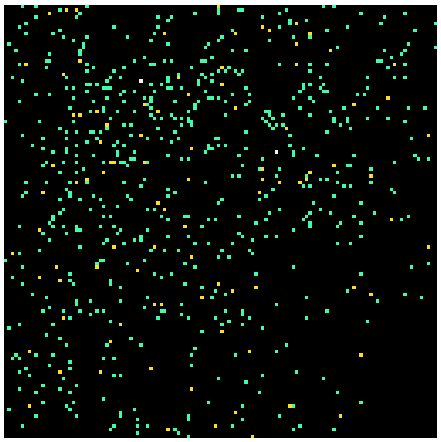

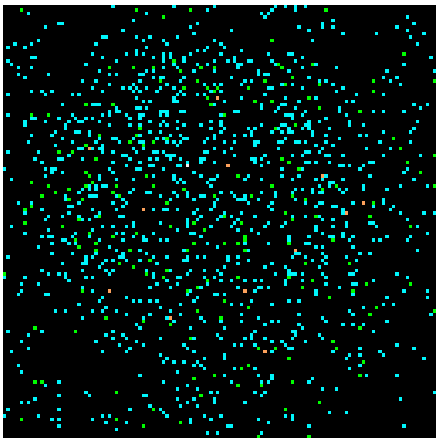

Figure 9. Overall spectra image of ruthenium and nickel inside the nanoparticle.

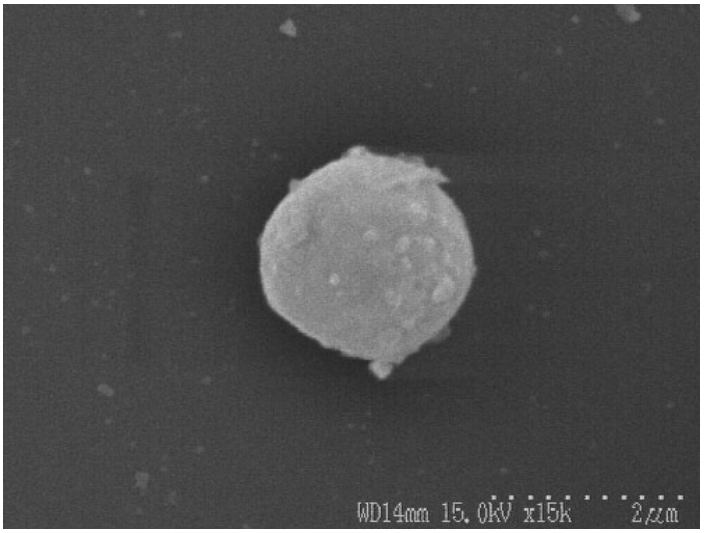

Figure 10. SEM image of the binary nanoparticle with synthesized with conditions similar to the one shown in Figure 7.

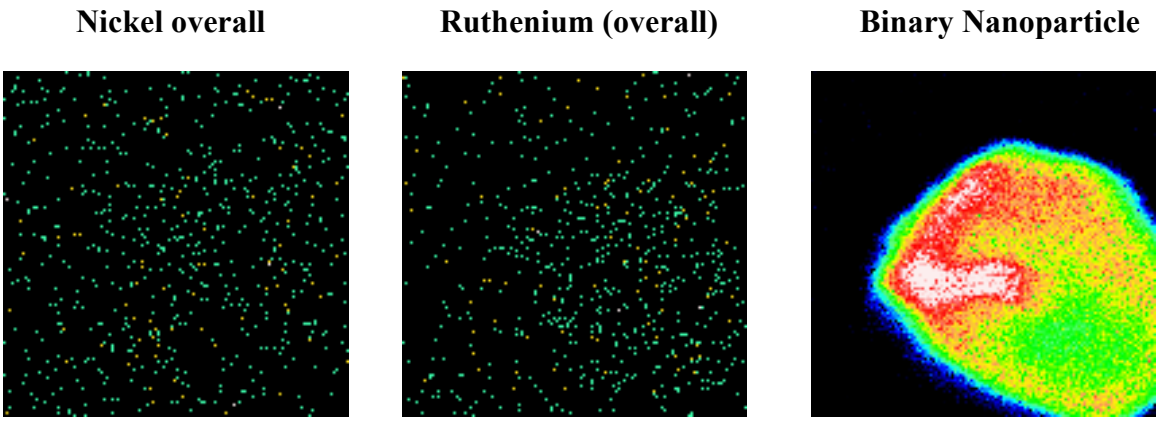

Figure 11. X-ray image of binary nanoparticle shown in Figure 10. It can be observed that the ruthenium is deposited inside the core and nickel formed an outside shell of the particle. Ruthenium at the center takes the shape of the inner core which can be seen from the overall imaging of the nanoparticle towards the right side of the X-ray image.

Nickel at center **Ruthenium at center**

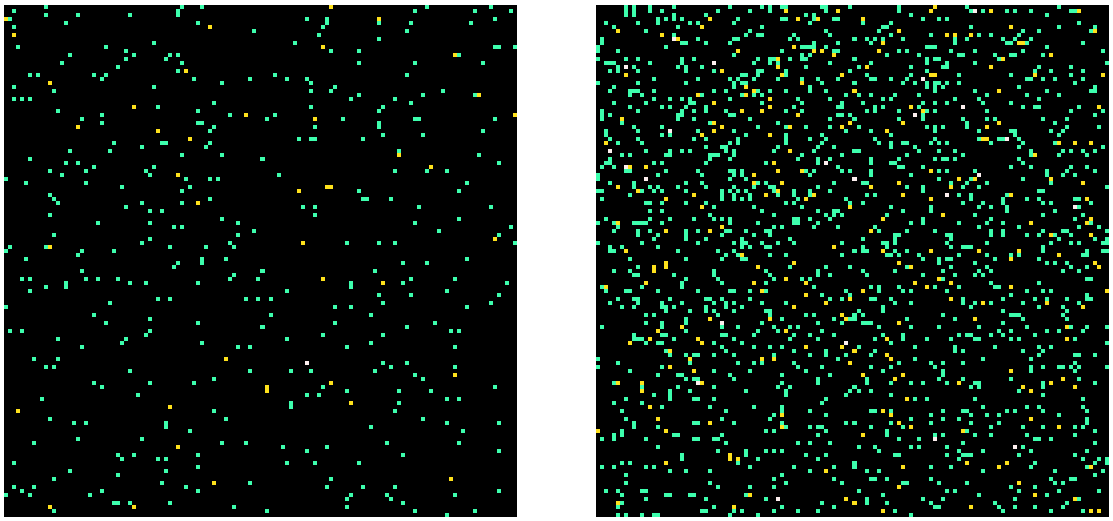

Figure 12. X-ray imaging of the binary nanoparticle at a center point inside the core of the nanoparticle. It can be observed that the population of ruthenium particles is more than the nickel nanoparticles.

Figure 13. Spectra image of the overall nanoparticle shown in Figure 7. This confirms the presence of ruthenium and nickel inside the binary nanoparticle.